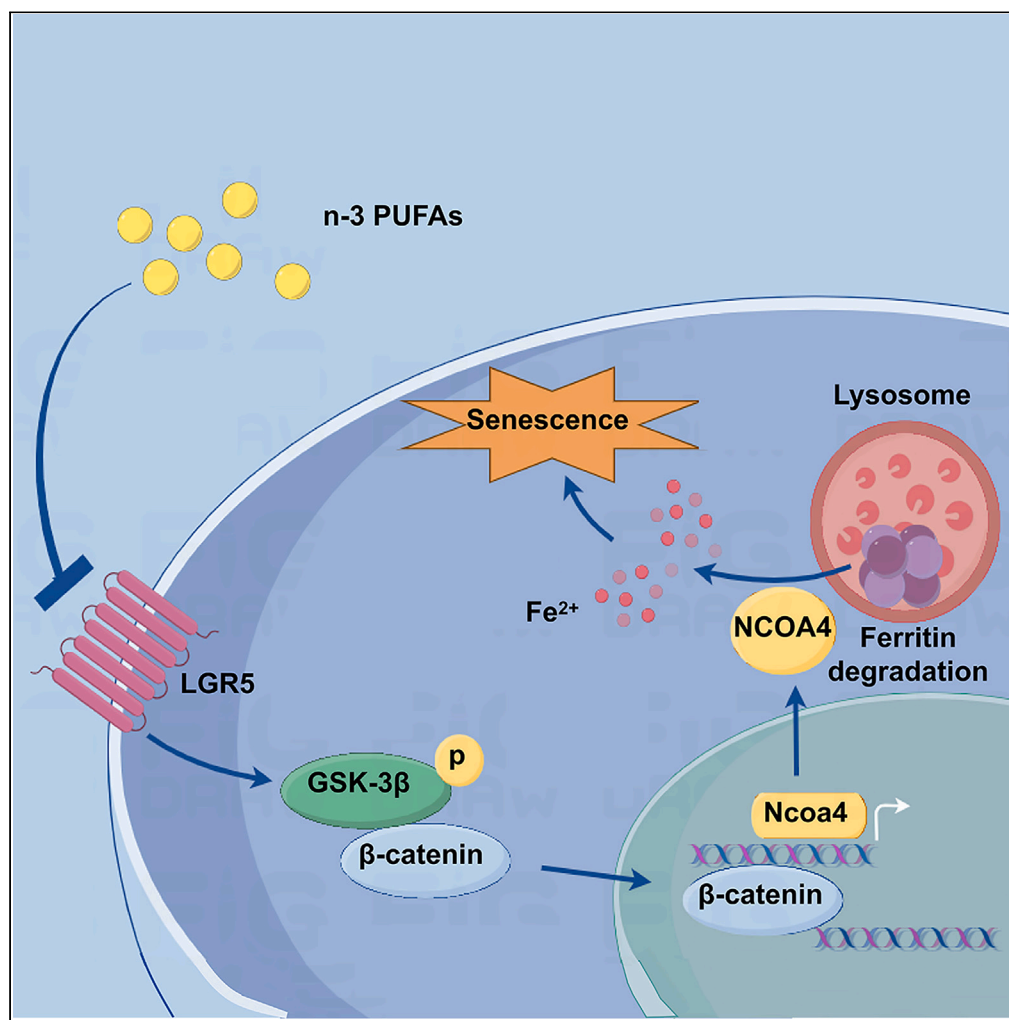


Article

n-3 polyunsaturated fatty acids delay intervertebral disc degeneration by inhibiting nuclear receptor coactivator 4-mediated iron overload



Xiang Ao, Tao Jiang, Yuan Li, ..., Liang Wang, Minjun Huang, Zhongmin Zhang

hmjlceb@163.com (M.H.)
nfzzm@163.com (Z.Z.)

Highlights

The increased ratio of endogenous n-3/n-6 PUFAs delay IVDD progression

n-3 PUFAs inhibit iron overload-mediated senescence of IVD cells

n-3 PUFAs reduce free iron content by inhibiting NCOA4-mediated ferritin degradation

n-3 PUFAs inhibit NCOA4 expression by inactivating the LGR5/β-catenin pathway

Article

n-3 polyunsaturated fatty acids delay intervertebral disc degeneration by inhibiting nuclear receptor coactivator 4-mediated iron overload

Xiang Ao,^{1,4} Tao Jiang,^{1,4} Yuan Li,^{2,3} Weiyi Lai,^{2,3} Zhengnan Lian,^{2,3} Liang Wang,^{2,3} Minjun Huang,^{2,3,*} and Zhongmin Zhang^{1,5,*}

SUMMARY

n-3 polyunsaturated fatty acids (PUFAs) are closely related to the progression of numerous chronic inflammatory diseases, but the role of n-3 PUFAs in the intervertebral disc degeneration (IVDD) remains unclear. In this study, male C57BL/6 wildtype mice (WT group, n = 30) and fat-1 transgenic mice (TG group, n = 30) were randomly selected to construct the IVDD model. The results demonstrated that the optimized composition of PUFAs in the TG mice had a significant impact on delaying IVDD and cellular senescence of intervertebral disc (IVD). Mechanismly, n-3 PUFAs inhibited IVD senescence by alleviating NCOA4-mediated iron overload. NCOA4 overexpression promoted iron overload and weakened the pro-proliferation and anti-senescence effect of DHA on the IVD cells. Furthermore, this study further revealed n-3 PUFAs downregulated NCOA4 expression by inactivating the LGR5/ β -catenin signaling pathway. This study provides an important theoretical basis for preventing and treating IVDD and low back pain.

INTRODUCTION

Low back pain (LBP) is a common clinical disease with a mean point prevalence of 12% and a lifetime prevalence of approximately 40%.¹ According to the Global Burden of Disease Study, LBP is the leading cause of years lived with disability.² The total annual medical costs associated with LBP in the United States exceed \$625 billion. Intervertebral disc degeneration (IVDD) is an important pathological basis for LBP, but early intervention methods for IVDD are still lacking.³

Dietary factors are closely related to IVDD.⁴⁻⁶ Among them, polyunsaturated fatty acids (PUFAs) are important nutrients. According to different structures and metabolites, PUFAs are mainly divided into the following categories: n-3 and n-6. The former such as docosahexaenoic acid (DHA) or eicosapentaenoic acid (EPA), which mainly plays an anti-inflammatory role; the latter mainly plays the pro-inflammatory role.⁷ A Mendelian randomization study showed a putative causal relationship between plasma n-3 PUFA levels and risk of LBP.⁸ Napier et al. reported that dietary supplementation with n-3 PUFAs could upregulate plasma n-3 PUFA levels and delay annulus fibrosus puncture-induced IVDD in rats.⁹ The above evidence suggests that n-3 PUFAs play an important role in IVDD, but the specific role and molecular mechanism of n-3 PUFAs on IVDD have not been fully elucidated.

Recent studies have shown that cellular senescence is a key factor in IVDD. Cellular senescence refers to the irreversible growth cycle arrest of cells, but the cells still secrete inflammatory factors, chemokines and proteolytic enzymes, further promoting the senescence of surrounding cells.¹⁰ Studies have shown that the expression of senescence markers, such as p16^{INK4A} and p53, is significantly increased in degenerated intervertebral disc (IVD).¹¹ Patil et al. showed that the specific elimination of p16^{INK4A}-positive senescent cells can effectively alleviate IVDD, suggesting that cellular senescence can be an important target for preventing IVDD.¹² Previous studies have shown that n-3 PUFAs significantly inhibited the cellular senescence and tissue aging.^{13,14} However, the relationship between n-3 PUFAs and senescence of the IVD cells still unknown.

Iron plays a crucial role in maintaining physiological homeostasis.¹⁵ However, an excess of free iron can activate oxidative stress through the Fenton reaction. This iron-dependent oxidative stress triggers a unique form of programmed cell death called ferroptosis.^{16,17} Previous study has demonstrated a significant increase in free iron content within degenerated IVD.¹⁸ Iron overload has been found to greatly enhance ferroptosis and expedite the process of IVDD.^{19,20} Furthermore, it is worth noting that cellular senescence is significantly influenced by oxidative stress caused by iron overload.^{21,22} Masaldan et al. revealed the iron content in senescent cells was found to be 30 times higher than normal.²³ *In vitro* study has shown that iron overload promoted the cellular senescence of chondrocytes.²⁴ However, the relationship between

¹Division of Spine Surgery, Department of Orthopaedics, Nanfang Hospital of Southern Medical University, Guangzhou, Guangdong, P.R. China

²Department of Spine Surgery, Center for Orthopedic Surgery, The Third Affiliated Hospital of Southern Medical University, Guangzhou, Guangdong, P.R. China

³Academy of Orthopaedics-Guangdong Province, Guangzhou, Guangdong, P.R. China

⁴These authors contributed equally

⁵Lead contact

*Correspondence: hmjlceb@163.com (M.H.), nfzzm@163.com (Z.Z.)

<https://doi.org/10.1016/j.isci.2023.108721>



Table 1. The content of n-3 and n-6 PUFAs and the ratio of n-6/n-3 PUFAs in IVD

		WT 18M	TG 18M	p value
IVD	n-6 PUFAs%	18.89 ± 1.67	17.03 ± 1.34	0.176
	n-3 PUFAs%	3.05 ± 0.30	5.18 ± 0.30 *	0.001
	n-6/n-3	6.21 ± 0.22	3.29 ± 0.15 *	0.000

Compared with the mice in the WT 18M group, the IVDs of the mice in the TG 18M group contained higher n-3 PUFAs content, lower n-6 PUFAs content, and significantly lower n-6/n-3 PUFAs ratio.

IVD: intervertebral disc degeneration; PUFA: polyunsaturated fatty acid; TG: transgenic; WT: wild type.

iron overload and senescence of IVD remains unclear. Generally, iron is stored in ferritin, a protein complex consisting of 24 ferritin light chains (FTL) and ferritin heavy chains 1 (FTH1), which converts ferrous ions to ferric ions. The conversion results in an inert deposition of iron and an elimination of iron toxicity.²⁵ When the iron content is insufficient, ferritin is bound by nuclear receptor coactivator 4 (NCOA4) and delivered to autophagolysosomes for the degradation and release of iron.^{26–28} A study showed that the expression of NCOA4 is significantly increased in degenerated IVD, indicating that NCOA4-mediated ferritin degradation and iron overload are closely related to cellular senescence in IVD.²⁹ Additionally, n-3 PUFAs have been found to alleviate various types of tissue degeneration caused by iron overload, such as liver fibrosis and retinal degeneration.^{30,31}

In this study, we employed fat-1 transgenic (TG) mice that possess a desaturase enzyme encoded by the fat-1 gene. This enzyme has the ability to convert n-6 PUFAs to n-3 PUFAs within the body. To investigate the effect and mechanism of n-3 PUFAs in regulating iron homeostasis and cellular senescence in the progression of IVDD, we constructed an aged (18-month-old) mouse IVDD model and extracted primary IVD cells for *in vivo* and *in vitro* analysis.³² Additionally, we explored the regulatory role of the leucine-rich-repeat-containing G-protein-coupled receptor 5 (LGR5)/β-catenin signaling pathway in this process.

RESULTS

Increased n-3 polyunsaturated fatty acids content and decreased n-6/n-3 polyunsaturated fatty acids ratio in transgenic mice

The results of gas chromatography were shown in Table 1. Compared with the C57BL6 wildtype (WT) mice, the IVDs of the fat-1 transgenic (TG) mice contained higher n-3 PUFAs content ($5.18 \pm 0.30\%$ vs. $3.05 \pm 0.30\%$, $p = 0.001$), lower n-6 PUFAs content ($17.03\% \pm 1.34\%$ vs. $18.89\% \pm 1.67\%$, $p = 0.176$), and significantly lower n-6/n-3 PUFAs ratio (3.29 ± 0.15 vs. 6.21 ± 0.22 , $p < 0.001$). The above results indicated that TG mice can optimize the PUFAs content through the endogenous pathway and downregulate the n-6/n-3 PUFAs ratio in the body.

Delayed progression of intervertebral disc degeneration in transgenic mice

The results of histological staining were shown in Figures 1A and 1B. Compared with the Ctrl group, the mice of WT 18M group exhibited higher degree of IVDD, which was manifested as nucleus pulposus (NP) fissure formation, annulus fibrosus (AF) rupture, NP invasion and a significant decrease in the cartilage endplate (CEP) height (Figure 1C). However, the IVD structure of the mice in TG 18M group remained intact, and the CEP height was significantly higher than that of the WT 18M group. Safranin O/Fast Green (SO/FG) staining results demonstrated that chondrogenesis of NP, lack of distinct boundary between the NP/AF region and ossification of CEP occurred in the mice of WT 18M group. In contrast, less above degenerative changes were occurred in the mice of TG 18M group. The histological scoring based on histological staining showed that compared with the Ctrl group, the mice of WT 18M group exhibited significantly higher degeneration scores, while the degeneration scores of the mice in TG 18M group were significantly lower than that in the WT 18M group (Figure 1D). In addition, the results of Masson staining also confirmed that the matrix degradation of IVD tissue in 18-month-old TG mice was reduced compared with the contemporary WT mice (Figure S1).

Matrix metabolism is an important indicator of IVDD (Figures 1E and 1F). The IHC results showed that compared with the Ctrl group, the mice of WT 18M group exhibited decreased expression of Col2a1, but significantly increased matrix metalloproteinase-13 (MMP-13)- and Osteocalcin (OCN)-positive cell ratio in AF (Figures 1G and 1H). The proportion of Collagen X-positive cells in the CEP was also significantly increased in the mice of WT 18M group (Figure 1I). However, the expression of Col2a1 was increased, and the positive cell ratios of Collagen X, MMP-13 and OCN were significantly decreased in the mice of TG 18M group.

n-3 polyunsaturated fatty acids inhibit cellular senescence in intervertebral disc

Cellular senescence is a key factor of IVDD. Therefore, the degree of cellular senescence in IVD was evaluated. IHC results showed that compared with the mice in Ctrl group, the significantly higher p53- and p16^{INK4A}-positive cell ratios were observed in the IVD of the mice in the WT 18M group. However, the positive cell ratios of p53 and p16^{INK4A} were significantly decreased in the IVD of the mice in the TG 18M group (Figures 2A–2F).

The rat primary IVD (NP and AF) cells were extracted for *in vitro* experiments. IL-1β (10 ng/ml) was exogenous added to mimic the inflammatory environment of IVDD. The results of the CCK-8 assay showed the proliferation of NP and AF cells were significantly decreased after the

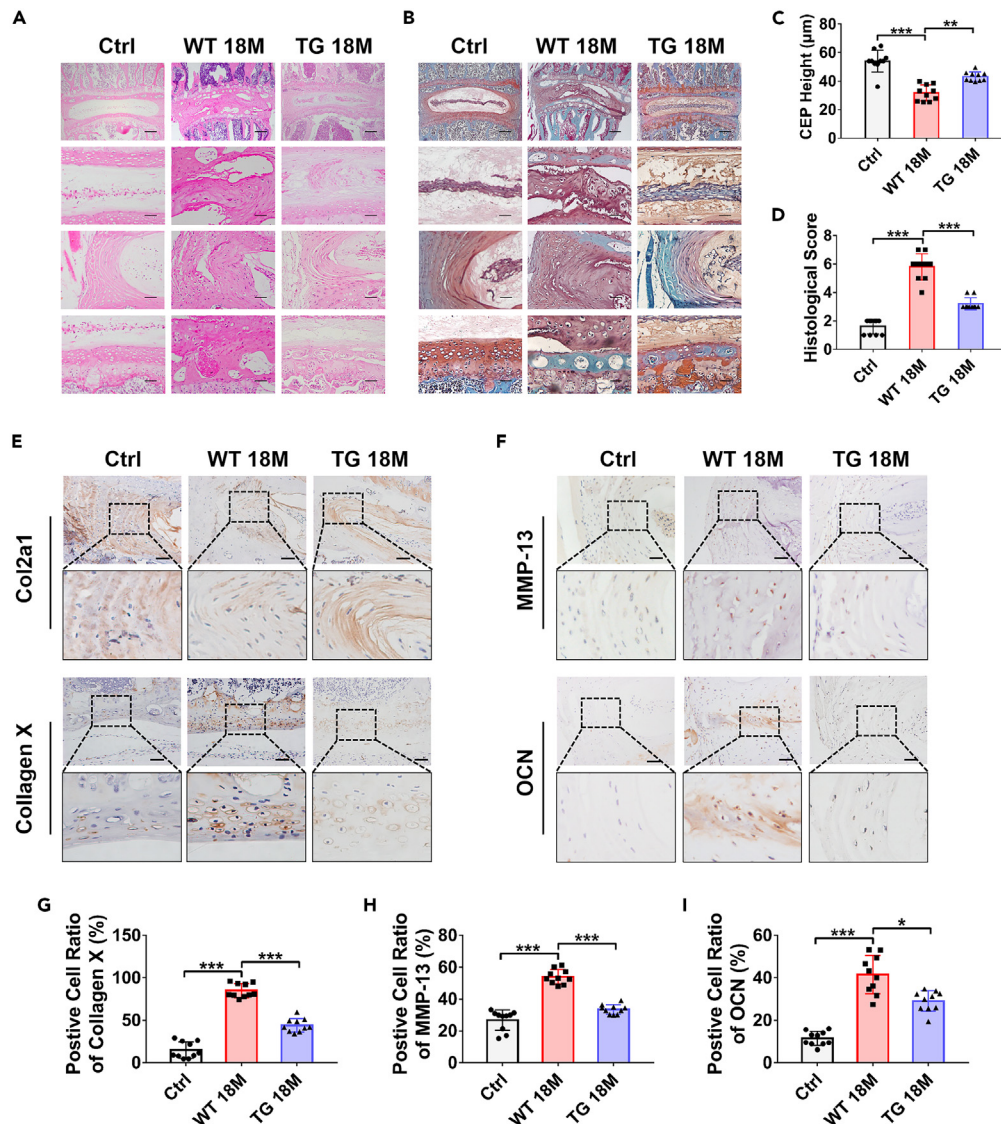


Figure 1. Histological staining and IHC results of the IVD of mice in each group

(A) H&E staining results of IVD in the mice of each group. Compared to the Ctrl group mice, WT 18M group mice exhibited marked IVD tissue destruction, whereas the morphology of IVD in the TG 18M group mice was basically maintained.
 (B) Safranin O/fast green staining results of IVD in the mice of each group.
 (C) Statistical results of CEP height in the mice of each group.
 (D) Statistical results of IVDD histological scoring in the mice of each group.
 (E) IHC results of Col2a1 and Collagen X in the IVD of mice in each group.
 (F) IHC results of MMP-13 and OCN in the IVD of mice in each group.
 (G) Statistical results of the positive cell ratio for Collagen X.
 (H) Statistical results of the positive cell ratio for MMP-13. I: Statistical results of the positive cell ratio for OCN. * represents $p < 0.05$, ** represents $p < 0.01$, *** represents $p < 0.001$. Statistical analysis was performed with one-way ANOVA followed by LSD. Scale bar = $50\mu\text{m}$ or $200\mu\text{m}$ (A, B) and $50\mu\text{m}$ (E). Data are represented as mean \pm SD.

treatment of IL-1 β , while the exogenous addition of DHA significantly promoted the proliferation of NP and AF cells, and 1 nM DHA caused the optimal effect (Figures 2G and 2H). Next, the NP cells and AF cells were treated with 1 nM DHA for 24, 48, and 72 h. The results showed that the pro-proliferation effects of DHA on IVD cells were positively correlated with the treatment duration (Figures 2I and 2J). Therefore, DHA (1 nM and 72 h) was used in the subsequent experiments. The results of Senescence-associated β -galactosidase (SA- β -gal) staining showed IL-1 β significantly increased the positive cell ratio in the NP and AF cells. The exogenous addition of DHA could effectively reduce the SA- β -gal-positive cell in the IL-1 β -treated NP cells and AF cells (Figures 2K–2M). The qRT-PCR results indicated the mRNA expression of biomarkers of

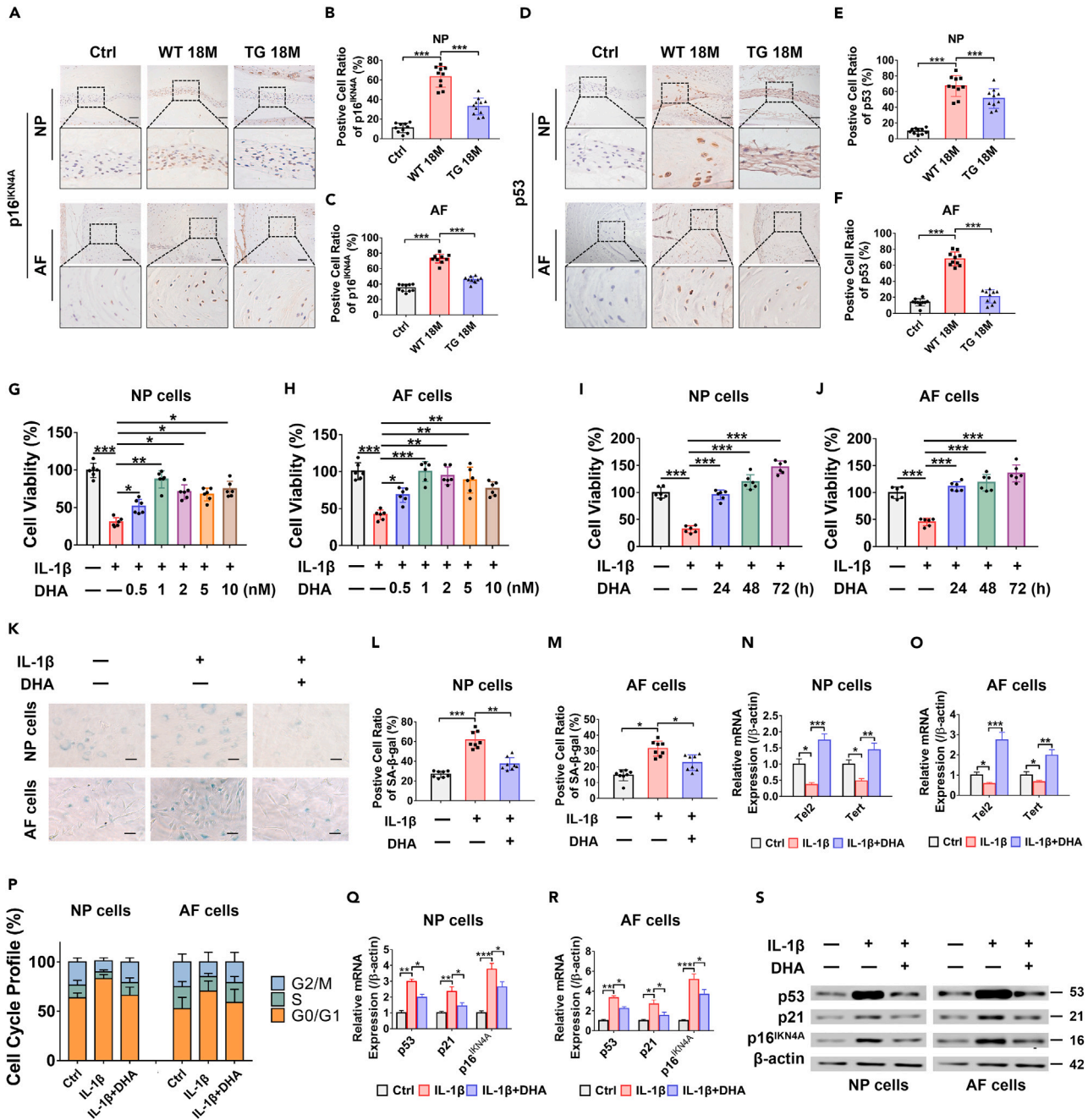


Figure 2. n-3 PUFAs inhibit cellular senescence in IVD

(A) IHC results of p16^{INK4A} in NP and AF of mice in each group.

(B and C) Statistical results of the positive cell ratio of p16^{INK4A} in NP and AF.

(D) IHC results of p53 in NP and AF of mice in each group.

(E and F) Statistical results of the positive cell ratio for p53.

(G–J) The results of the CCK-8 assay demonstrated that treatment with 1nM DHA for 72 h had the most significant effect in promoting the proliferation of NP and AF cells.

(K) SA-β-gal staining results of NP cells and AF cells treated with IL-1β or IL-1β plus DHA.

(L and M) Statistical results of the SA-β-gal-positive cell ratio in the NP cells and AF cells.

(N and O) mRNA expression of Tel2 and Tert in NP cells and AF cells were detected using qRT-PCR.

(P) The results of the cell cycle detection demonstrated that IL-1β increased the proportion of G0/G1 phase, while decreasing the proportion of S phase and G2/M phase in NP and AF cells. DHA was found to effectively block the effect of IL-1β.

Figure 2. Continued

(Q and R) mRNA expression of p53, p21, p16^{INK4A} in NP cells and AF cells were detected using qRT-PCR.

(S) Western blot analyses of p53, p21, p16^{INK4A} protein expression in NP cells and AF cells treated with IL-1 β or IL-1 β plus DHA. * represents $p < 0.05$, ** represents $p < 0.01$, *** represents $p < 0.001$. Statistical analysis was performed with one-way ANOVA followed by LSD. Scale bar = 50 μ m (A, D) or 20 μ m (K). Data are represented as mean \pm SD.

telomere activity (Tel2, Tert) was significantly decreased in IL-1 β -treated NP and AF cells, while significantly increased after the addition of DHA (Figures 2N and 2O). The results of the cell cycle detection demonstrated that IL-1 β increased the proportion of G0/G1 phase, while decreasing the proportion of S phase and G2/M phase in NP and AF cells. DHA was found to effectively block the effect of IL-1 β (Figure 2P). Moreover, the mRNA expression of the senescence markers p53, p21 and p16^{INK4A} was significantly increased in IL-1 β -treated NP and AF cells, while significantly decreased after the exogenous addition of DHA (Figures 2Q and 2R). The protein expression levels of p53, p21 and p16^{INK4A} were also increased in the NP and AF cells after the treatment of IL-1 β , while the exogenous addition of DHA significantly reduced the expression of these proteins in the IL-1 β -treated IVD cells (Figure 2S).

n-3 polyunsaturated fatty acids affect intervertebral disc senescence by alleviating iron overload

Iron overload is an important pathological factor leading to cellular senescence. Hence the free iron content (mg/g prot) in IVD tissues was detected. The results showed that compared with the Ctrl group, the free iron content in the IVDs of the mice in WT 18M group was significantly increased, while the free iron content of the mice in TG 18M group was significantly lower than that in the WT 18M group (Figure 3A). *In vitro*, the results showed IL-1 β significantly increased the free iron contents in the NP and AF cells, while DHA significantly reduced the free iron content in IL-1 β -treated IVD cells (Figures 3B and 3C). Iron overload can lead to the lipid peroxidation and production of MDA. The results of MDA content assay showed that IL-1 β significantly increased the MDA contents in NP and AF cells, while DHA significantly reduced the MDA contents in the IL-1 β -treated IVD cells (Figures 3D and 3E). A ferrous ion probe (FerroOrange) was used to stained ferrous ions in cells, and the mean fluorescence intensity (MFI) was calculated. The results showed the amount of ferrous ions was significantly increased in the NP and AF cells after the treatment of IL-1 β , and DHA could significantly reduce the amount of ferrous ions (Figures 3F–3H). Transmission electron microscopy (TEM) results revealed that mitochondrias in NP and AF cells treated with IL-1 β were smaller and denser compared to the control group. However, these changes were effectively reversed by DHA treatment (Figure 3I). Additionally, the results of ROS fluorescence staining demonstrated that DHA successfully inhibited the IL-1 β -induced increase in ROS levels in NP and AF cells (Figures 3J–3L). Subsequently, we investigated the correlation between iron overload and cell senescence in IVD. The Western blot results showed the increased protein expression of p53, p21 and p16^{INK4A} in the NP and AF cells induced by IL-1 β could be effectively inhibited by the iron chelator DFO (Figure 3M). On the other hand, the results of Western blot and PCR experiments showed additional iron supplementation with FAC weakened the inhibitory effect of DHA on the expression of p53, p21, and p16^{INK4A} in the IL-1 β -treated NP and AF cells (Figures 3N–3P). Then, the cell cycle detection showed the addition of FAC promotes the cell-cycle arrest (Figure 3Q). The results of SA- β -gal staining further confirmed that the iron chelator DFO significantly decreased the senescent NP and AF cells induced by IL-1 β , while additional FAC could weaken the inhibitory effect of DHA on the cellular senescence (Figures 3R–3T). The above results suggest that iron overload is an important mechanism that mediates the effect of DHA on the senescence of IVD.

n-3 polyunsaturated fatty acids inhibit iron overload by regulating the nuclear receptor coactivator 4-mediated ferritin degradation

NCOA4-mediated degradation of ferritin is an important source of free iron. The immunofluorescence (IF) staining results showed that compared with the mice in Ctrl group, the expression of ferritin in the IVD of mice in WT 18M group was significantly lower, while the ferritin-positive cell ratio in the IVD of the mice in TG 18M group was significantly higher than that of WT 18M group (Figures 4A and 4B). The IHC results showed the positive cell ratio of NCOA4 in the IVD of the mice in WT 18M group was significantly higher than that of Ctrl mice, while significantly lower in the mice of TG 18M group than that of WT 18M group (Figures 4C and 4D). IL-1 β up-regulated the mRNA expression of Fth1 and NCOA4 (Figures 4E and 4F), while the protein expression of ferritin in the IL-1 β -treated NP and AF cells was reduced (Figure 4G), indicated that the degradation of ferritin was aggravated in the progression of IVDD. Continually, the NP and AF cells overexpressing NCOA4 were constructed by transfection (Figure 4H). The results of IF colocalization experiments demonstrated the colocalization staining of Ferritin and the autophagosome marker LC3B in the IL-1 β -treated NP and AF cells increased, while the colocalization decreased after the exogenous addition of DHA (Figure 4I). Moreover, overexpression of NCOA4 also increased the free iron content (Figures 4J–4N), and inhibited the proliferation in the NP and AF cells (Figures 4O and 4P). Western blot results showed that the overexpression of NCOA4 could effectively block the effect of DHA on inhibiting the protein expression of p53, p21 and p16^{INK4A} in NP and AF cells (Figure 4Q). The above results indicate that NCOA4 is a key factor in the regulation of iron overload in IVDD and is an important target of n-3 PUFA in delaying the iron overload-induced IVD senescence.

n-3 polyunsaturated fatty acids inhibit nuclear receptor coactivator 4 expression by regulating the Wnt/ β -catenin signaling pathway

Wnt/ β -catenin signaling pathway is closely related to cellular senescence of IVD, but the relationship between Wnt/ β -catenin signaling pathway and iron overload in IVD is unclear. The IHC results for the IVD tissue showed that compared with the mice in Ctrl group, the

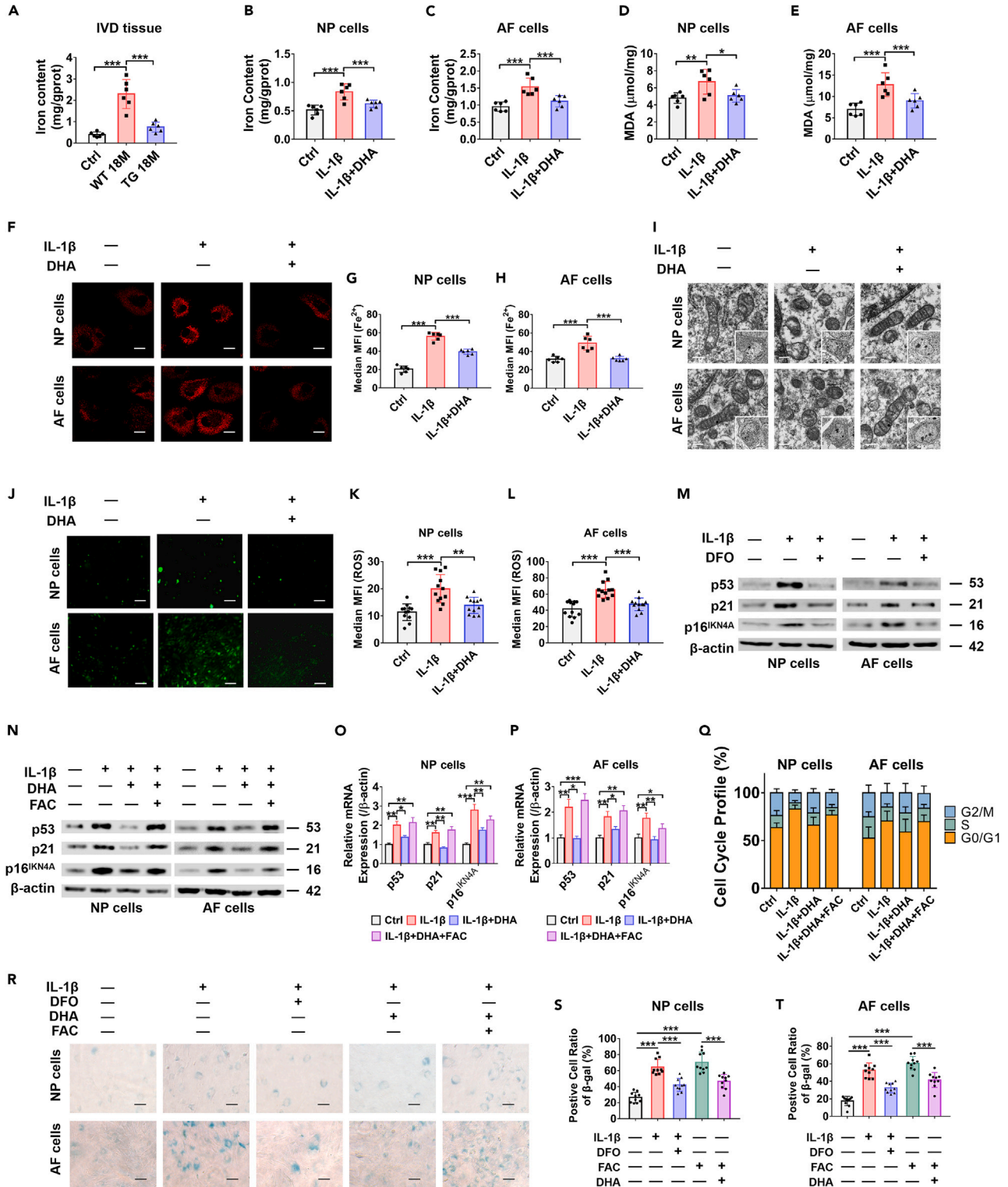


Figure 3. n-3 PUFAs regulated IVD senescence by mediating iron overload

(A) Compared with the Ctrl group mice, the free iron content in IVD tissues of mice in the WT 18M group was significantly increased, and that of mice in the TG 18M group was significantly lower than that of mice in the WT 18M group.

(B and C) Statistical results of free iron content in NP cells and AF cells treated with IL-1β or IL-1β plus DHA.

Figure 3. Continued

- (D and E) MDA content assay of the NP cells and AF cells treated with IL-1 β or DHA.
(F) FerroOrange staining results of NP cells and AF cells treated with IL-1 β or IL-1 β plus DHA.
(G and H) Statistical results of FerroOrange mean fluorescence intensity of NP cells and AF cells.
(I) TEM results revealed that mitochondria in NP and AF cells treated with IL-1 β were observed to be smaller and denser compared to the control group, the changes were effectively reversed by DHA treatment.
(J) the results of ROS fluorescence staining demonstrated that DHA successfully inhibited the IL-1 β -induced increase in ROS levels.
(K and L) Statistical results of mean fluorescence intensity of ROS in NP cells and AF cells.
(M) Western blot analyses of p53, p21, p16^{INK4A} protein expression in NP cells and AF cells treated with IL-1 β or IL-1 β plus DFO.
(N) Western blot analyses of p53, p21, p16^{INK4A} protein expression in NP cells and AF cells treated with IL-1 β , IL-1 β plus DHA or IL-1 β plus DHA and FAC.
(O and P) mRNA expression of p53, p21, p16^{INK4A} in NP cells and AF cells were detected using qRT-PCR.
(Q) The results of cell cycle detection showed that the exogenous addition of FAC increased the proportion of G0/G1 phase, and decreased the proportion of S phase and G2/M phase in the NP and AF cells.
(R) SA- β -gal staining of the NP cells and AF cells treated with IL-1 β , DFO, FAC or DHA.
(S and T) Statistical results of the SA- β -gal-positive cell ratio in NP cells and AF cells. * represents $p < 0.05$, ** represents $p < 0.01$, *** represents $p < 0.001$. Statistical analysis was performed with one-way ANOVA followed by LSD. Scale bar = 2 μ m (F), 20 μ m (J, R) or 200nm (I). Data are represented as mean \pm SD.

mice in WT 18M group exhibited an increased nuclear expression of β -catenin in IVD, while the expression of β -catenin in the IVD of the TG 18M group mice mainly occurred in the cytoplasm (Figure 5A). The results of IF staining showed increased nuclear translocation of β -catenin in IL-1 β -treated NP and AF cells, and the exogenous addition of DHA effectively inhibited the nuclear translocation of β -catenin (Figures 5B–5D). Furthermore, the Western blot results showed that after the treatment of IL-1 β , the phosphorylation of GSK-3 β and the nuclear translocation of β -catenin were upregulated in the NP and AF cells, while this effect was inhibited by the addition of DHA (Figure 5E). The mRNA expression of the β -catenin downstream targets C-myc and Cyclin-D1 were significantly increased in the IL-1 β -treated NP cells and AF cells, while decreased after the treatment of DHA (Figures 5F and 5G). The above results suggest that DHA can effectively block the activation of the Wnt/ β -catenin signaling pathway in IVDD.

Then the NP and AF cells were treated with Wnt agonist (CAS-853220-52). The addition of Wnt agonist weakened the effect of DHA on the protein expression of NCOA4 and Ferritin in the IL-1 β -treated NP and AF cells (Figure 5H). Additionally, Wnt agonist also weakened the effect of DHA on free iron content in the IL-1 β -treated NP and AF cells (Figures 5I and 5J). FerroOrange staining showed that Wnt agonist could effectively block the inhibitory effect of DHA on the amount of ferrous iron in NP cells and AF cells (Figures 5K–5M). The above results indicate that the Wnt/ β -catenin signaling pathway is the key mechanism that mediates PUFA to inhibit iron overload in the progression of IVDD.

Leucine-rich-repeat-containing G-protein-coupled receptor 5 is involved in n-3 polyunsaturated fatty acids regulation of the Wnt/ β -catenin signaling pathway

LGR5, also known as G-protein-coupled receptor 49, is a membrane protein that plays an important role in regulating the activity of the Wnt/ β -catenin signaling pathway. IHC results showed that the LGR5-positive cell ratio in IVD of the mice in WT 18M group was significantly higher than that in the Ctrl group, and the LGR5-positive cell ratio of the mice in TG 18M group was significantly lower than that of the WT 18M group (Figures 6A and 6B). In *in vitro* experiments, Western blot results revealed the exogenous addition of DHA significantly reduced the up-regulation of LGR5 in the IL-1 β -treated NP cells and AF cells (Figure 6C). Then, LGR5 was overexpressed by plasmid transfection. Western blot results showed that LGR5 overexpression up-regulated the nucleus expression of β -catenin in the NP and AF cells treated with IL-1 β and DHA (Figure 6D). IF results also confirmed that the overexpression of LGR5 promotes the nuclear translocation of β -catenin (Figures 6E–6G) and the mRNA expression of C-myc and Cyclin-D1 (Figures 6H and 6I). We further explored the relationship between LGR5 and downstream iron overload and cellular senescence in IVD cells. The results of the FerroOrange staining showed that overexpressing LGR5 could significantly block the effect of DHA on the amount of ferrous iron in IL-1 β -treated NP cells and AF cells, which could be inhibited by the Wnt/ β -catenin signaling pathway inhibitor XAV-939 (Figure 6J–6L). In addition, the Western blot results showed that LGR5 overexpression could significantly inhibit the effect of DHA on the protein expression of p53, p21, and p16^{INK4A}, this effect was significantly blocked by XAV-939 (Figure 6M).

DISCUSSION

A Mendelian randomization study confirmed a putative causal relationship between plasma levels of n-3 PUFAs and risk of LBP.⁸ Sanders et al. reported that the content of circulating n-3 PUFAs was negatively correlated with the incidence of LBP, and the effect was independent of the inhibition of systemic inflammation by n-3 PUFAs, suggesting that n-3 PUFAs are closely related to IVDD.³³ To our knowledge, this is the first study that utilized *fat-1* TG mice to demonstrate that elevated levels of endogenous n-3 PUFAs and optimized composition of n-6/n-3 PUFAs significantly inhibit IVDD. Exogenous addition of DHA can inhibit NCOA4-mediated ferritin degradation and alleviate iron overload and cellular senescence in IVD cells by regulating the LGR5/ β -catenin signaling pathway. This study provides a new theoretical basis for the prevention and treatment of IVDD and LBP.

PUFAs are mainly divided into the following categories: n-3 and n-6. Recent studies have shown that the effect of PUFAs mainly depends on the n-6/n-3 ratio rather than the content of certain PUFAs.^{34,35} The results of gas chromatographic analysis showed that compared with that of the WT 18M mice, the content of n-3 PUFAs was significantly increased, while the content of n-6 PUFAs was only slightly decreased in the

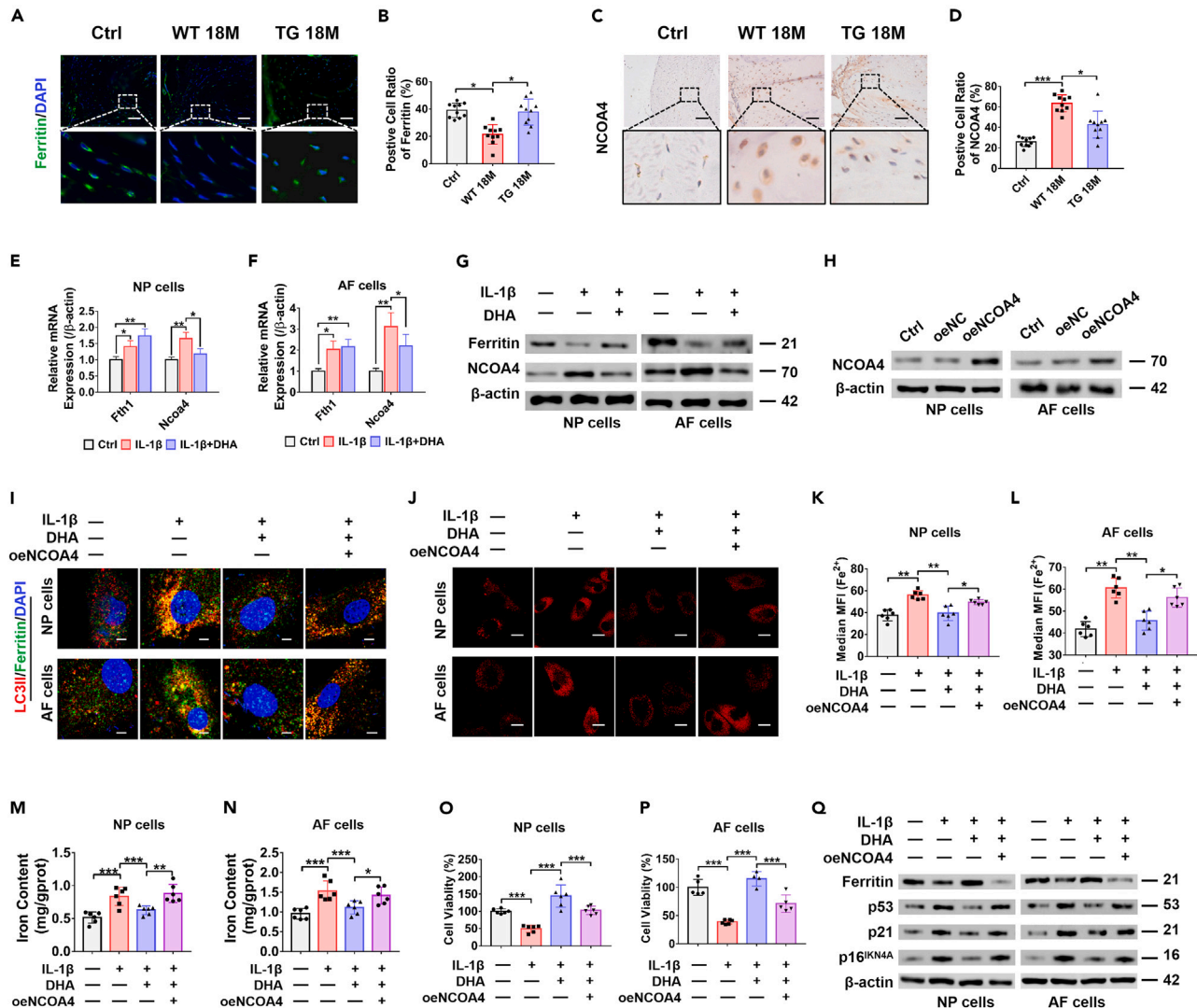


Figure 4. n-3 PUFAs inhibit NCOA4-mediated degradation of ferritin

(A) IF results of Ferritin in IVD of mice in each group.
 (B) Statistical results of the positive cell ratio of Ferritin.
 (C) IHC results of NCOA4 in IVD of mice in each group.
 (D) Statistical results of the positive cell ratio of NCOA4.
 (E and F) mRNA expression of Fth1 and Ncoa4 in NP cells and AF cells were detected using qRT-PCR.
 (G) Western blot analyses of Ferritin and NCOA4 protein expression in NP cells and AF cells treated with IL-1β or IL-1β plus DHA.
 (H) NCOA4 over-expression of NP cells and AF cells after transfection was detected by Western blot analysis.
 (I) The IF results showed that compared with the Ctrl group, increased colocalization of Ferritin and LC3II was observed in IL-1β-treated NP cells and AF cells, and exogenous addition of DHA effectively inhibit this effect. However, overexpression of NCOA4 significantly blocked the effect of DHA.
 (J) FerroOrange staining results showed that the addition of Wnt agoist could effectively block the downregulation of DHA on the content of ferrous iron in NP and AF cells.
 (K and L) Statistics of FerroOrange mean fluorescence intensity of NP cells and AF cells.
 (M and N) Statistical results of free iron content in NP cells and AF cells treated with IL-1β, IL-1β plus DHA or IL-1β plus DHA with overexpression of NCOA4.
 (O and P) The results of CCK-8 assay showed that overexpression of NCOA4 significantly blocked the effect of DHA on the proliferation of NP cells and AF cells.
 (Q) Western blot analyses of Ferritin, p53, p21, p16^{INK4A} protein expression in NP cells and AF cells treated with IL-1β, IL-1β plus DHA or IL-1β plus DHA with overexpression of NCOA4. * represents p < 0.05, ** represents p < 0.01, *** represents p < 0.001. Statistical analysis was performed with one-way ANOVA followed by LSD. Scale bar = 50µm (A, C), 2µm (I) and 5µm (J). Data are represented as mean ± SD.

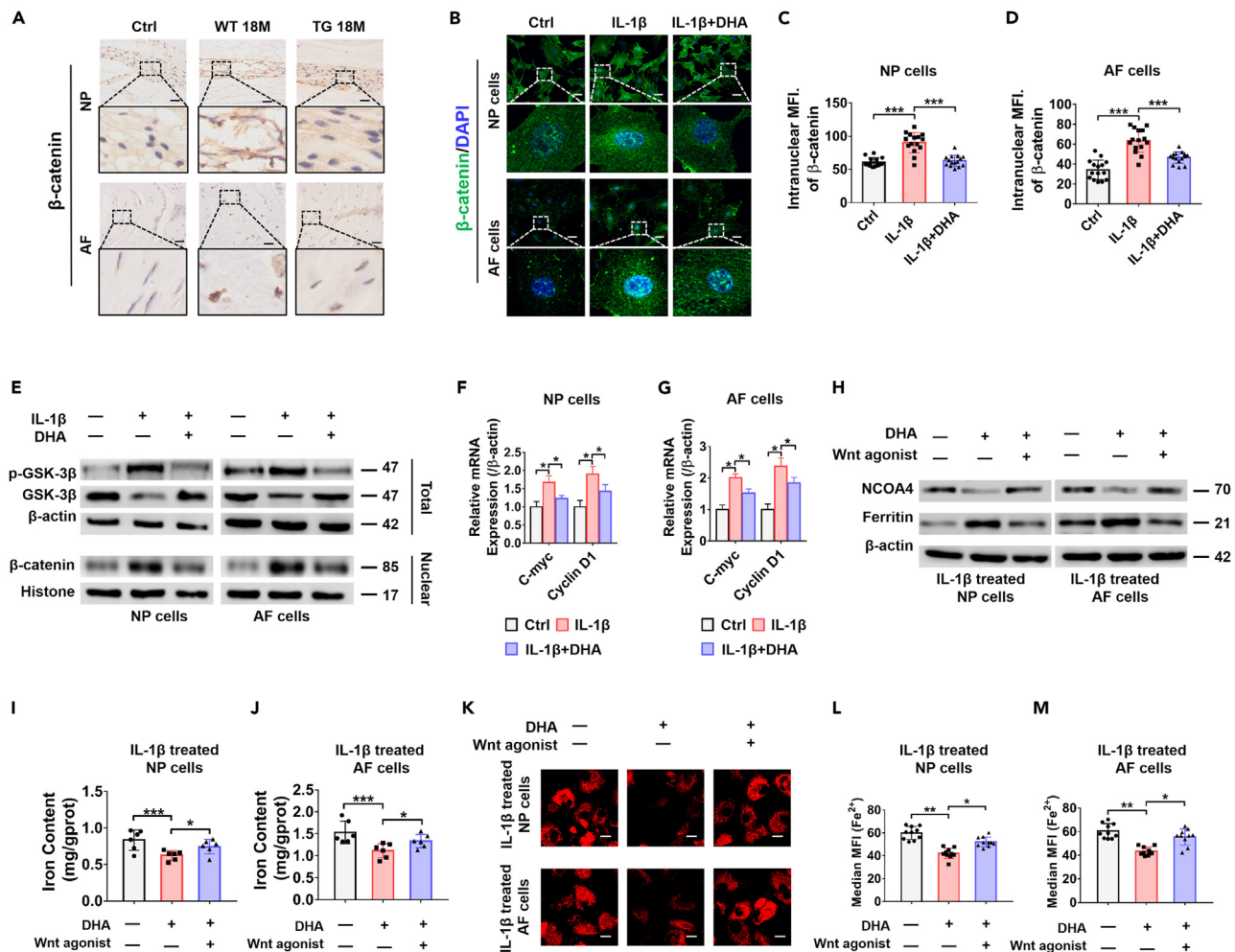


Figure 5. n-3 PUFAs inhibit NCOA4-mediated iron overload of IVD cells by regulating the Wnt/ β -catenin signaling pathway

(A) IHC results showed that compared with the Ctrl group mice, the nuclear expression of β -catenin increased in the IVD of the WT 18M group mice, while β -catenin mainly expressed in the cytoplasm of IVD cells in the TG 18M group mice.

(B) IF results showed that compared with the Ctrl group, nuclear transport of β -catenin in NP cells and AF cells increased, while the exogenous addition of DHA effectively inhibited β -catenin translocation into the nucleus.

(C and D) Statistical results of the intranuclear MFI of β -catenin in the NP and AF cells.

(E) Western blot results showed that the phosphorylation of GSK-3 β and the nuclear translocation of β -catenin increased in NP cells and AF cells treated with IL-1 β , and the above effects were inhibited by the exogenous addition of DHA.

(F and G) mRNA expression of C-myc and Cyclin-D1 in NP cells and AF cells treated with IL-1 β or IL-1 β plus DHA.

(H) Western blot analyses of Ferritin and NCOA4 protein expression in NP cells and AF cells treated with IL-1 β , IL-1 β plus DHA or IL-1 β plus DHA with Wnt agonist.

(I and J) Statistical results of free iron content in NP cells and AF cells treated with IL-1 β , IL-1 β plus DHA or IL-1 β plus DHA with Wnt agonist.

(K) FerroOrange staining results showed that the addition of Wnt agonist effectively blocked the downregulation of DHA on the content of ferrous iron in NP and AF cells.

(L and M) Statistics of FerroOrange mean fluorescence intensity of NP cells and AF cells. * represents $p < 0.05$. Statistical analysis was performed with one-way ANOVA followed by LSD. Scale bar = 50 μ m (A), 20 μ m (B) and 5 μ m (K). Data are represented as mean \pm SD.

IVD tissue of TG 18M mice; however, the ratio of n-6/n-3 PUFAs in TG 18M mice was significantly reduced, and the degree of IVDD was significantly reduced, indicating that the composition of endogenous PUFAs is closely related to IVDD. Clinical studies have shown that due to changes in lifestyle and dietary habits, the ratio of n-6/n-3 PUFAs in humans is much higher than the recommended value (2.5–4/1); hence, supplementation with n-3 PUFAs can optimize the ratio of n-6/n-3 PUFAs and delay numerous pathological processes.^{36,37} Cellular senescence is a key factor that is involved in IVDD. Previous studies have revealed the inhibitory effect of n-3 PUFAs on endothelial cellular senescence, but the effect of n-3 PUFAs on IVD senescence has not been reported. This study confirmed for the first time that n-3 PUFAs significantly inhibited the expression of senescence markers (p53, p21, p16^{INK4A}), reduced SA- β -gal-positive cells and promoted cell proliferation in IVD, indicating that n-3 PUFAs alleviated IVDD mainly by promoting cell viability and inhibiting cellular senescence. The results

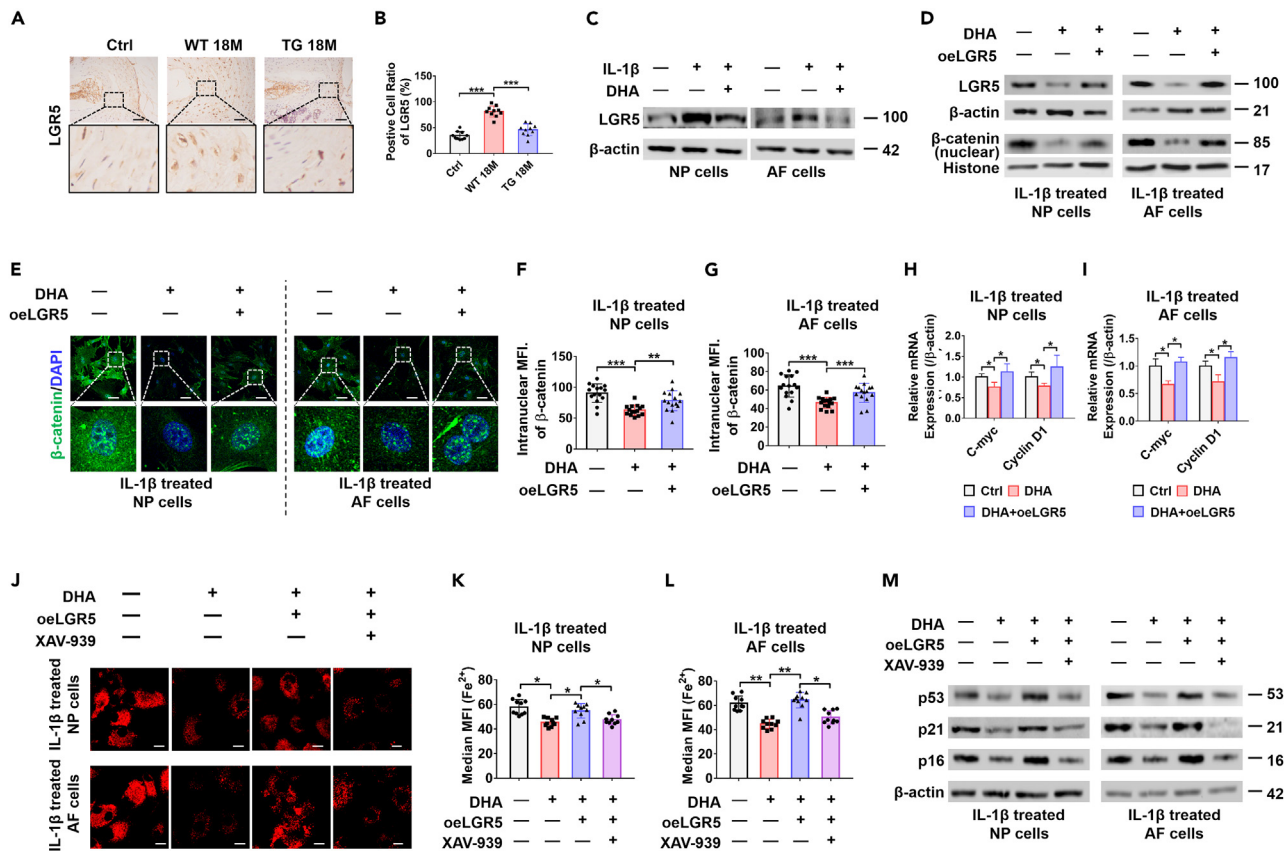


Figure 6. n-3 PUFAs regulates Wnt/β-catenin signaling pathway by inhibiting LGR5 expression

(A) IHC results of LGR5 in IVD of mice in each group.
 (B) Statistical results of the positive cell ratio for LGR5.
 (C) Western blot analyses of LGR5 protein expression in NP cells and AF cells treated with IL-1β or IL-1β plus DHA.
 (D) Western blot results showed that overexpression of LGR5 effectively blocked the inhibitory effect of DHA on the nuclear translocation of β-catenin in IL-1β-treated NP cells and AF cells.
 (E) IF results showed that overexpression of LGR5 blocked the inhibitory effect of DHA on the nuclear translocation of β-catenin in NP and AF cells.
 (F and G) Statistical results of the intranuclear MFI of β-catenin in the NP and AF cells.
 (H and I) mRNA expression of C-myc and Cyclin-D1 in NP cells and AF cells treated with IL-1β, IL-1β plus DHA or IL-1β plus DHA with overexpression of LGR5.
 (J) FerroOrange staining results showed that overexpression of LGR5 could effectively block the downregulation of DHA on the content of ferrous iron in NP and AF cells, while the Wnt pathway inhibitor XAV-939 effectively inhibited the effect of LGR5 overexpression.
 (K and L) Statistics of FerroOrange mean fluorescence intensity of NP cells and AF cells.
 (M) Western blot results showed that overexpression of LGR5 could effectively block the inhibitory effect of DHA on the expression of p53, p21 and p16^{INK4A} in NP and AF cells, and XAV-939 could effectively inhibit the effects of LGR5 overexpression. * represents $p < 0.05$, ** represents $p < 0.01$, *** represents $p < 0.001$. Statistical analysis was performed with one-way ANOVA followed by LSD. Scale bar = 50μm (A), 20μm (E) and 2μm (J). Data are represented as mean ± SD.

of CCK-8 showed that, compared with that of 1 nM DHA, the effect of a higher concentration of DHA on the proliferation of IVD cells was decreased. A previous study showed that a large intake of DHA can become the main source of inflammatory factors, and excessive inflammatory stimulation significantly inhibits the proliferation and function of IVD cells.³⁸ This provides further support that the key to improving physiological homeostasis of PUFAs lies in maintaining an appropriate ratio of n-6/n-3 PUFAs rather than the absolute value of PUFA content.

Clinical studies have shown that serum n-3 PUFAs are positively correlated with ferritin content, while n-6 PUFAs are negatively correlated with ferritin content, suggesting that supplementing n-3 PUFAs and optimizing the n-6/n-3 PUFA ratio have important roles in maintaining iron homeostasis in IVDs.^{39,40} The results of this study showed that n-3 PUFAs significantly reduced the free iron content and MDA level in the IVDs, suggesting that n-3 PUFAs inhibited iron overload in the IVDs. PCR and Western blot results showed that DHA significantly inhibited the expression of NCOA4 and the degradation of ferritin. Immunohistochemical results also confirmed the expression of NCOA4 decreased and the expression of ferritin increased in the IVD of TG 18M mice in comparison with the WT 18M mice. Overexpression of NCOA4 significantly blocked the inhibitory effect of DHA on iron overload in the IVD cells. The above results suggest that n-3 PUFAs inhibit iron overload in the IVDs by inhibiting NCOA4-mediated ferritin degradation. Iron overload is closely related to cellular senescence, and the results of this study showed that the free iron content in IVD was increased significantly with the progression of IVDD, which was consistent with a previous

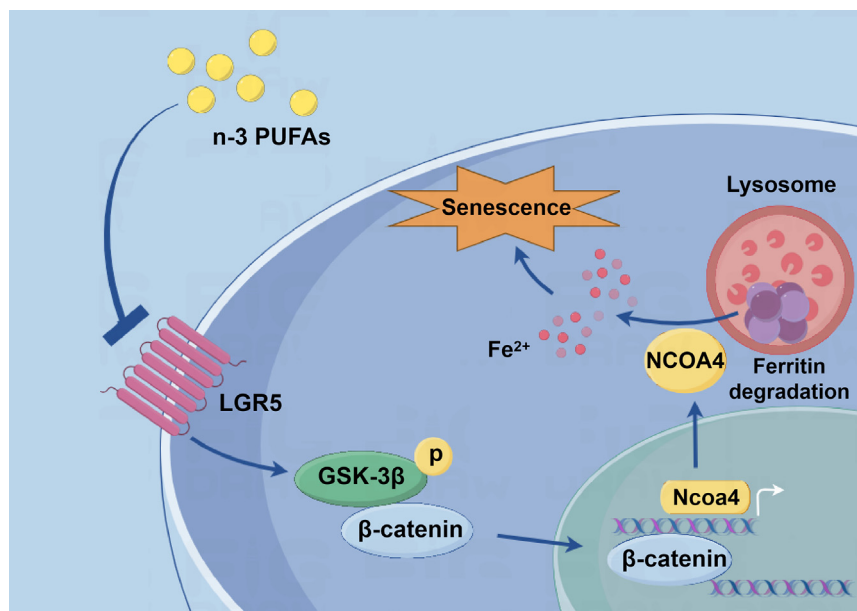


Figure 7. Schematic diagram of the regulatory effects of n-3 PUFAs on IVD senescence

n-3 PUFAs exert their inhibitory effects by reducing LGR5 expression, suppressing GSK-3 β phosphorylation and β -catenin nuclear transport, decreasing NCOA4 expression and preventing ferritin degradation. This leads to a reduction in free iron content and ultimately inhibits IVD cell senescence and IVDD.

study.¹⁸ Supplementation of FAC or overexpression of NCOA4-induced iron overload significantly increased the expression of p53, p21, p16 and the SA- β -Gal-positive ratio in IVD cells, whereas exogenous addition of iron chelator DFO significantly inhibited cellular senescence. Therefore, n-3 PUFAs downregulate NCOA4 expression, inhibit iron overload and IVD senescence, which may be an important mechanism for n-3 PUFAs to regulate IVDD.

To further explore the regulatory mechanism of n-3 PUFAs on NCOA4, we examined the role of the LGR5/ β -catenin signaling pathway in the regulation of n-3 PUFAs in IVD senescence. LGR5 belongs to the rhodopsin-like family and is a transmembrane protein that is easily regulated by dietary factors.⁴¹ The results of this study confirmed that the expression of LGR5 was significantly increased in IVDD, while n-3 PUFAs significantly downregulated the expression of LGR5. LGR5 is an important upstream signal of β -catenin, and LGR5 overexpression effectively promoted the nuclear transport of β -catenin in IVD cells.⁴² In addition, compared with the WT 18M mice, the nuclear transport of β -catenin in the IVD of TG 18M mice was reduced. At the same time, *in vitro* experiments confirmed that DHA inhibited the nuclear transport of β -catenin in the IVDs and decreased the mRNA expression of its downstream transcription factors C-myc and Cyclin-D1. The above results confirmed that n-3 PUFAs can inhibit the activity of LGR5/ β -catenin signaling pathway in IVD. β -catenin plays an important role in IVD senescence, but its relationship to IVD iron overload is unclear.⁴³ Santana-Codina et al. reported that the β -catenin downstream transcription factor C-myc can promote ferritin degradation and iron accumulation.²⁶ The results of this study indicated that the exogenous addition of Wnt agonists could significantly upregulate NCOA4 expression and increase free iron levels in IVD cells. Furthermore, overexpressing LGR5 or adding a Wnt agonist could significantly block the inhibitory effect of DHA on IVD senescence. These results suggest that n-3 PUFA downregulates NCOA4 expression and suppresses iron overload and cellular senescence in IVD by modulating the LGR5/ β -catenin signaling pathway (Figure 7).

In conclusion, by utilizing *fat-1* TG mice and extracting mouse primary IVD cells, we confirmed that n-3 PUFAs could regulate the activity of the LGR5/ β -catenin signaling pathway, inhibit NCOA4-mediated ferritin degradation and iron overload, and alleviate IVD senescence and degeneration. This study provides an important theoretical basis for the prevention and treatment of IVDD and LBP.

Limitations of the study

This study has the following limitations. First, only DHA was used in the *in vitro* experiments, and the effects and mechanisms of other important n-3 PUFAs, such as eicosapentanoic acid (EPA), on IVDD are still unclear. Previous studies have shown that n-3 PUFA supplementation in the form of EPA:DHA (6:1) is more effective.^{44,45} Therefore, the specific effects of different n-3 PUFAs on IVD senescence and degeneration need to be further explored. Second, it is unknown whether n-3 PUFAs, as a macromolecular substance, affects IVD senescence through direct replacement with the cell membrane, through changing the relevant properties of the membrane, or through some key metabolites. In follow-up experiments, we will further screen the membrane receptors of n-3 PUFAs or explore the specific metabolites and molecular mechanisms of n-3 PUFAs that affect IVD homeostasis through metabolomics to provide a new theoretical basis for the clinical application of n-3 PUFAs and the prevention of IVDD.

STAR★METHODS

Detailed methods are provided in the online version of this paper and include the following:

- **KEY RESOURCES TABLE**
- **RESOURCE AVAILABILITY**
 - Lead contact
 - Materials availability
 - Data and code availability
- **EXPERIMENTAL MODEL AND STUDY PARTICIPANT DETAILS**
 - Mouse model of IVDD
- **METHOD DETAILS**
 - Histochemistry, immunohistochemical staining and tissue quantitative analysis
 - Cell culture and treatment
 - Cell counting kit-8 (CCK-8) assay
 - Cell cycle detection
 - SA-β-gal staining
 - Free iron content assay
 - Malondialdehyde (MDA) content assay
 - Cytofluorescence assay
 - TEM assay
 - qRT-PCR
 - Western blot
- **QUANTIFICATION AND STATISTICAL ANALYSIS**

SUPPLEMENTAL INFORMATION

Supplemental information can be found online at <https://doi.org/10.1016/j.isci.2023.108721>.

ACKNOWLEDGMENTS

We thank Xinggui Tian and Linrui Jiang MD, of the Academy of Orthopedics, Guangdong Province, Guangzhou, Guangdong, P.R. China, for their technical support on the histology and immunohistochemistry. This work was funded by National Key R&D Program of China (2022YFC25029004 [ZZ]), the National Natural Sciences Foundation of China (82072520 [ZZ]), the Natural Science Foundation of Guangdong Province (2019A1515012074 [MH]), Guangdong Basic and Applied Basic Research Foundation (2021A1515010005).

This work was performed at the Academy of Orthopedics, Guangdong Province, Guangzhou, Guangdong, P.R. China.

AUTHOR CONTRIBUTIONS

Conceptualization, M.H., L.W., and Z.Z.; methodology, X.A., T.J., and Z.L.; software, Y.L.; validation, X.A., Z.L., and M.Z.; formal analysis, L.J.; investigation, X.A.; resources, Z.L.; data curation, T.J. and Y.L.; writing—original draft preparation, X.A.; writing—review and editing, M.H.; funding acquisition, M.H., Z.Z., and T.C. All authors have read and agreed to the published version of the article.

DECLARATION OF INTERESTS

All authors declare no competing financial interests.

Received: August 18, 2023

Revised: October 24, 2023

Accepted: December 11, 2023

Published: December 13, 2023

REFERENCES

1. Hoy, D., Bain, C., Williams, G., March, L., Brooks, P., Blyth, F., Woolf, A., Vos, T., and Buchbinder, R. (2012). A systematic review of the global prevalence of low back pain. *Arthritis Rheum.* 64, 2028–2037.
2. GBD 2017 DALYs and HALE Collaborators, Degu, A., Kalkidan, H., Solomon, A., Cristiana, A., Nooshin, A., Hedayat, A., Foad, A., Jemal, A., Ahmed, A., et al. (2018). Global, regional, and national disability-adjusted life-years (DALYs) for 359 diseases and injuries and healthy life expectancy (HALE) for 195 countries and territories, 1990–2017: a systematic analysis for the Global Burden of Disease Study 2017. *Lancet* 392, 1859–1922.
3. Cheng, Z., Xiang, Q., Wang, J., and Zhang, Y. (2021). The potential role of melatonin in retarding intervertebral disc ageing and degeneration: A systematic review. *Ageing Res. Rev.* 70, 101394.
4. Liao, Z., Luo, R., Li, G., Song, Y., Zhan, S., Zhao, K., Hua, W., Zhang, Y., Wu, X., and Yang, C. (2019). Exosomes from mesenchymal stem cells modulate endoplasmic reticulum stress to protect against nucleus pulposus cell death and

- ameliorate intervertebral disc degeneration in vivo. *Theranostics* 9, 4084–4100.
5. Xu, X., Wang, D., Zheng, C., Gao, B., Fan, J., Cheng, P., Liu, B., Yang, L., and Luo, Z. (2019). Progerin accumulation in nucleus pulposus cells impairs mitochondrial function and induces intervertebral disc degeneration and therapeutic effects of sulforaphane. *Theranostics* 9, 2252–2267.
 6. Zhang, X., Chen, J., Huang, B., Wang, J., Shan, Z., Liu, J., Chen, Y., Li, S., Fan, S., and Zhao, F. (2019). Obesity Mediates Apoptosis and Extracellular Matrix Metabolic Imbalances via MAPK Pathway Activation in Intervertebral Disk Degeneration. *Front. Physiol.* 10, 1284.
 7. Custers, Emma, E.M., Kiliaan, and Amanda, J. (2022). Dietary lipids from body to brain. *Prog. Lipid Res.* 85, 101144.
 8. Zhou, S., Zhu, G., Xu, Y., Gao, R., Li, H., Han, G., Su, W., and Wang, R. (2022). Mendelian Randomization Study on the Putative Causal Effects of Omega-3 Fatty Acids on Low Back Pain. *Front. Nutr.* 9, 819635.
 9. NaPier, Z., Kanim, L.E.A., Arabi, Y., Salehi, K., Sears, B., Perry, M., Kim, S., Sheyn, D., Bae, H.W., and Glaeser, J.D. (2019). Omega-3 Fatty Acid Supplementation Reduces Intervertebral Disc Degeneration. *Med. Sci. Monit.* 25, 9531–9537.
 10. Wu, J., Chen, Y., Liao, Z., Liu, H., Zhang, S., Zhong, D., Qiu, X., Chen, T., Su, D., Ke, X., et al. (2022). Self-amplifying loop of NF- κ B and periostin initiated by PIEZO1 accelerates mechano-induced senescence of nucleus pulposus cells and intervertebral disc degeneration. *Mol. Ther.* 30, 3241–3256.
 11. Shi, S., Kang, X.J., Zhou, Z., He, Z.M., Zheng, S., and He, S.S. (2022). Excessive mechanical stress-induced intervertebral disc degeneration is related to Piezo1 overexpression triggering the imbalance of autophagy/apoptosis in human nucleus pulposus. *Arthritis Res. Ther.* 24, 119.
 12. Patil, P., Dong, Q., Wang, D., Chang, J., Wiley, C., Demaria, M., Lee, J., Kang, J., Niedernhofer, L.J., Robbins, P.D., et al. (2019). Systemic clearance of p16INK4a-positive senescent cells mitigates age-associated intervertebral disc degeneration. *Aging Cell* 18, e12927.
 13. Qureshi, A.W., Altamimy, R., El Habhab, A., El Itawi, H., Farooq, M.A., Zobairi, F., Hasan, H., Amoura, L., Kasseem, M., Auger, C., et al. (2020). Ageing enhances the shedding of splenocyte microvesicles with endothelial pro-senescent effect that is prevented by a short-term intake of omega-3 PUFA EPA:DHA 6:1. *Biochem. Pharmacol.* 173, 113734.
 14. Chi, D.H., Kahyo, T., Islam, A., Hasan, M.M., Waliullah, A.S.M., Mamun, M.A., Nakajima, M., Ikoma, T., Akita, M., Maekawa, Y., et al. (2022). NAD⁺ Levels Are Augmented in Aortic Tissue of ApoE^{-/-} Mice by Dietary Omega-3 Fatty Acids. *Arterioscler. Thromb. Vasc. Biol.* 42, 395–406.
 15. Killilea, D.W., Wong, S.L., Cahaya, H.S., Atamna, H., and Ames, B.N. (2004). Iron accumulation during cellular senescence. *Ann. N. Y. Acad. Sci.* 1019, 365–367.
 16. Liu, Y., and Gu, W. (2022). p53 in ferroptosis regulation: the new weapon for the old guardian. *Cell Death Differ.* 29, 895–910.
 17. Sharma, A., and Flora, S.J.S. (2021). Positive and Negative Regulation of Ferroptosis and Its Role in Maintaining Metabolic and Redox Homeostasis. *Oxid. Med. Cell. Longev.* 2021, 9074206.
 18. Lu, S., Song, Y., Luo, R., Li, S., Li, G., Wang, K., Liao, Z., Wang, B., Ke, W., Xiang, Q., et al. (2021). Ferroportin-Dependent Iron Homeostasis Protects against Oxidative Stress-Induced Nucleus Pulposus Cell Ferroptosis and Ameliorates Intervertebral Disc Degeneration In Vivo. *Oxid. Med. Cell. Longev.* 2021, 6670497.
 19. Fan, C., Chu, G., Yu, Z., Ji, Z., Kong, F., Yao, L., Wang, J., Geng, D., Wu, X., and Mao, H. (2023). The role of ferroptosis in intervertebral disc degeneration. *Front. Cell Dev. Biol.* 11, 1219840.
 20. Zhu, J., Sun, R., Sun, K., Yan, C., Jiang, J., Kong, F., and Shi, J. (2023). The deubiquitinase USP11 ameliorates intervertebral disc degeneration by regulating oxidative stress-induced ferroptosis via deubiquitinating and stabilizing Sirt3. *Redox Biol.* 62, 102707.
 21. Noh, B., Blasco-Conesa, M.P., Rahman, S.M., Monga, S., Ritzel, R., Guzman, G., Lai, Y.J., Ganesh, B.P., Urayama, A., McCullough, L.D., and Moruno-Manchon, J.F. (2023). Iron overload induces cerebral endothelial senescence in aged mice and in primary culture in a sex-dependent manner. *Aging Cell* 22, e13977.
 22. Federti, E., Vinchi, F., Iatcenko, I., Ghigo, A., Matte, A., Toya, S.C.M., Siciliano, A., Chiabrando, D., Tolosano, E., Vance, S.Z., et al. (2023). Duality of Nr1f2 in iron-overload cardiomyopathy. *Haematologica* 108, 1335–1348.
 23. Masaldan, S., Clatworthy, S.A.S., Gamell, C., Meggyesy, P.M., Rigopoulos, A.T., Haupt, S., Haupt, Y., Denoyer, D., Adlard, P.A., Bush, A.I., and Cater, M.A. (2018). Iron accumulation in senescent cells is coupled with impaired ferritinophagy and inhibition of ferroptosis. *Redox Biol.* 14, 100–115.
 24. Karim, A., Bajbouj, K., Shafarin, J., Qaisar, R., Hall, A.C., and Hamad, M. (2022). Iron Overload Induces Oxidative Stress, Cell Cycle Arrest and Apoptosis in Chondrocytes. *Front. Cell Dev. Biol.* 10, 821014.
 25. Ajoalabady, A., Aslkhodapasandhokmabad, H., Libby, P., Tuomilehto, J., Lip, G.Y.H., Penninger, J.M., Richardson, D.R., Tang, D., Zhou, H., Wang, S., et al. (2021). Ferritinophagy and ferroptosis in the management of metabolic diseases. *Trends Endocrinol. Metab.* 32, 444–462.
 26. Santana-Codina, N., and Mancias, J.D. (2018). The Role of NCOA4-Mediated Ferritinophagy in Health and Disease. *Pharmaceuticals* 11, 114.
 27. Quiles Del Rey, M., and Mancias, J.D. (2019). NCOA4-Mediated Ferritinophagy: A Potential Link to Neurodegeneration. *Front. Neurosci.* 13, 238.
 28. Santana-Codina, N., Gikandi, A., and Mancias, J.D. (2021). The Role of NCOA4-Mediated Ferritinophagy in Ferroptosis. *Adv. Exp. Med. Biol.* 1301, 41–57.
 29. Yang, R.Z., Xu, W.N., Zheng, H.L., Zheng, X.F., Li, B., Jiang, L.S., and Jiang, S.D. (2021). Involvement of oxidative stress-induced annulus fibrosus cell and nucleus pulposus cell ferroptosis in intervertebral disc degeneration pathogenesis. *J. Cell. Physiol.* 236, 2725–2739.
 30. Helal, M.G., and El-Kashef, D.H. (2020). Krill oil alleviates oxidative stress, iron accumulation and fibrosis in the liver and spleen of iron-overload rats. *Environ. Sci. Pollut. Res. Int.* 27, 3950–3961.
 31. Liu, Y., Bell, B.A., Song, Y., Zhang, K., Anderson, B., Axelsen, P.H., Bohannon, W., Agbaga, M.P., Park, H.G., James, G., et al. (2022). Deuterated docosahexaenoic acid protects against oxidative stress and geographic atrophy-like retinal degeneration in a mouse model with iron overload. *Aging Cell* 21, e13579.
 32. Wang, W., Jing, X., Du, T., Ren, J., Liu, X., Chen, F., Shao, Y., Sun, S., Yang, G., and Cui, X. (2022). Iron overload promotes intervertebral disc degeneration via inducing oxidative stress and ferroptosis in endplate chondrocytes. *Free Radic. Biol. Med.* 190, 234–246.
 33. Sanders, A.E., Weatherspoon, E.D., Ehrmann, B.M., Soma, P.S., Shaikh, S.R., Preisser, J.S., Ohrbach, R., Fillingim, R.B., and Slade, G.D. (2022). Circulating Omega-6 and Omega-3 Polyunsaturated Fatty Acids in Painful Temporomandibular Disorder and Low Back Pain. *J. Pain* 23, 1724–1736.
 34. Simopoulos, A.P., Serhan, C.N., and Bazinet, R.P. (2021). The need for precision nutrition, genetic variation and resolution in Covid-19 patients. *Mol. Aspects Med.* 77, 100943.
 35. Wei, Y., Meng, Y., Li, N., Wang, Q., and Chen, L. (2021). The effects of low-ratio n-6/n-3 PUFA on biomarkers of inflammation: a systematic review and meta-analysis. *Food Funct.* 12, 30–40.
 36. Colombo, S.M., Parrish, C.C., and Wijekoon, M.P.A. (2018). Optimizing long chain-polyunsaturated fatty acid synthesis in salmonids by balancing dietary inputs. *PLoS One* 13, e0205347.
 37. Senftleber, N.K., Albrechtsen, A., Lauritzen, L., Larsen, C.L., Bjerregaard, P., Diaz, L.J., Rønn, P.F., and Jørgensen, M.E. (2020). Omega-3 fatty acids and risk of cardiovascular disease in Inuit: First prospective cohort study. *Atherosclerosis* 312, 28–34.
 38. Marventano, S., Kolacz, P., Castellano, S., Galvano, F., Buscemi, S., Mistretta, A., and Grosso, G. (2015). A review of recent evidence in human studies of n-3 and n-6 PUFA intake on cardiovascular disease, cancer, and depressive disorders: does the ratio really matter. *Int. J. Food Sci. Nutr.* 66, 611–622.
 39. Zhou, Y.E., Kubow, S., and Egeland, G.M. (2011). Is iron status associated with highly unsaturated fatty acid status among Canadian Arctic Inuit. *Food Funct.* 2, 381–385.
 40. Li, Z., Li, X., Zhang, Y., Feng, X., Yang, F., Su, D., Qiu, J., Ling, W., and Yang, Y. (2013). Erythrocyte membrane fatty acid composition is related to overloaded plasma ferritin in Chinese males with angiographic coronary artery disease. *Food Funct.* 4, 1535–1542.
 41. Chen, Y., Wang, M.H., Zhu, J.Y., Xie, C.F., Li, X.T., Wu, J.S., Geng, S.S., Han, H.Y., and Zhong, C.Y. (2020). TAp63 α targeting of Lgr5 mediates colorectal cancer stem cell properties and sulforaphane inhibition. *Oncogenesis* 9, 89.
 42. Yang, L., He, X., Jing, G., Wang, H., Niu, J., Qian, Y., and Wang, S. (2021). Layered Double Hydroxide Nanoparticles with Osteogenic Effects as miRNA Carriers to Synergistically Promote Osteogenesis of MSCs. *ACS Appl. Mater. Interfaces* 13, 48386–48402.
 43. Hao, Y., Ren, Z., Yu, L., Zhu, G., Zhang, P., Zhu, J., and Cao, S. (2022). p300 arrests intervertebral disc degeneration by

- regulating the FOXO3/Sirt1/Wnt/ β -catenin axis. *Aging Cell* 21, e13677.
44. Gaertner, S., Auger, C., Farooq, M.A., Pollet, B., Khemais-Benkhiat, S., Niazi, Z.R., Schrevers, S., Park, S.H., Toti, F., Stephan, D., and Schini-Kerth, V.B. (2020). Oral Intake of EPA:DHA 6:1 by Middle-Aged Rats for One Week Improves Age-Related Endothelial Dysfunction in Both the Femoral Artery and Vein: Role of Cyclooxygenases. *Int. J. Mol. Sci.* 21, 920.
 45. Belcastro, E., Rehman, A.U., Remila, L., Park, S.H., Gong, D.S., Anton, N., Auger, C., Lefebvre, O., Goetz, J.G., Collot, M., et al. (2021). Fluorescent nanocarriers targeting VCAM-1 for early detection of senescent endothelial cells. *Nanomedicine.* 34, 102379.
 46. Huang, M.J., Wang, L., Jin, D.D., Zhang, Z.M., Chen, T.Y., Jia, C.H., Wang, Y., Zhen, X.C., Huang, B., Yan, B., et al. (2014). Enhancement of the synthesis of n-3 PUFAs in fat-1 transgenic mice inhibits mTORC1 signalling and delays surgically induced osteoarthritis in comparison with wild-type mice. *Ann. Rheum. Dis.* 73, 1719–1727.
 47. Yang, F., Leung, V.Y.L., Luk, K.D.K., Chan, D., and Cheung, K.M.C. (2009). Injury-induced sequential transformation of notochordal nucleus pulposus to chondrogenic and fibrocartilaginous phenotype in the mouse. *J. Pathol.* 218, 113–121.

STAR★METHODS

KEY RESOURCES TABLE

REAGENT or RESOURCE	SOURCE	IDENTIFIER
Antibodies		
Mouse monoclonal anti-Col2a1	Millipore	Cat# MAB8887; RRID: AB_2260779
Rabbit polyclonal anti-MMP-13	ABclonal	Cat# A11755; RRID: AB_2758737
Rabbit polyclonal anti-OCN	ABclonal	Cat# A6205; RRID: AB_2766815
Rabbit polyclonal anti-NCOA4	ABclonal	Cat# A5695; RRID: AB_2766454
Rabbit polyclonal anti-LGR5	ABclonal	Cat# A12327; RRID: AB_2861654
Rabbit monoclonal anti-Collagen X	Abcam	Cat# ab260040; RRID: AB_3083555
Rabbit monoclonal anti-P16 ^{INK4A}	Abcam	Cat# ab241543; RRID: AB_2935877
Rabbit monoclonal anti-P53	Abcam	Cat# ab32049; RRID: AB_776982
Rabbit polyclonal anti-Ferritin	Abcam	Cat# ab75973; RRID: AB_1310222
Mouse monoclonal anti-LC3II	Abcam	Cat# ab243506; RRID: AB_2920656
Rabbit monoclonal anti-β-catenin	Abcam	Cat# ab223075; RRID: AB_3083545
Mouse monoclonal anti-β-actin	Abcam	Cat# ab8226; RRID: AB_306371
Mouse monoclonal anti-Histone	Abcam	Cat# ab1791; RRID: AB_302613
Goat anti-rabbit IgG HRP-linked Antibody	Abcam	Cat# ab205718; RRID: AB_2819160
Goat anti-mouse IgG HRP-linked Antibody	Abcam	Cat# ab205719; RRID: AB_2755049
Goat Anti-Rabbit IgG H&L (Alexa Fluor® 488)	Abcam	Cat# ab150077; RRID: AB_2630356
Goat Anti-Mouse IgG H&L (Alexa Fluor® 594)	Abcam	Cat# ab150116; RRID: AB_2650601
Bacterial and virus strains		
pcDNA3.1+NCOA4 (overexpression NCOA4)	Tsingke Biotech	N/A
pcDNA3.1+LGR5 (overexpression LGR5)	Tsingke Biotech	N/A
Chemicals, peptides, and recombinant proteins		
Hematoxylin dye	Sigma	HHS32
Eosin dye	Sigma	318906
L-glutamine	Sigma	G2150
Goat serum	Solarbio	SL038
DAPI	Solarbio	S2110
Collagenase type 2	Solarbio	9001-12-1
penicillin/streptomycin	Solarbio	P1400
Lipo3000	Invitrogen	L3000015
TRIzol reagent	Invitrogen	15596-018
Fetal bovine serum	Bovogen	SFBS-500
High-glucose Dulbecco's modified Eagle's medium	Gibco	C11965500BT
PrimeScript™ RT Master Mix Kit	Takara	RR00036A
TB Green™ Premix Ex Taq™ II	Takara	RR820A
Recombinant Murine IL-1β	Peprtech	211-11B
Docosahexaenoic acid	MCE	HY-B2167
Deferiprone	MCE	HY-B0568
Ferric ammonium citrate	MCE	HY-B1645
Wnt agonist	MCE	HY-114321
XAV-939	MCE	HY-15147

(Continued on next page)

Continued

REAGENT or RESOURCE	SOURCE	IDENTIFIER
<i>Critical commercial assays</i>		
CCK-8 reagent	Dojindo	CK04
Masson staining kit	Solarbio	G1340
Safranin O/Fast Green staining kit	Solarbio	G1371
SA- β -gal staining kit	Beyotime	C0602
Cell cycle assay kit	Beyotime	C1052
MDA content assay kit	Abbkine	S0131S
ROS Detection fluorometric assay kit	Abbkine	KTB1910
Iron content assay kit	Elabscience	E-BC-K881-M
<i>Oligonucleotides</i>		
qPCR primers for mRNA validation, Table S1	This paper	N/A
<i>Software and algorithms</i>		
Image J	NIH	N/A
SPSS	IBM	N/A
Graph pad	GraphPad	N/A

RESOURCE AVAILABILITY

Lead contact

Further information and requests for resources and reagents should be directed to and will be fulfilled by the lead contact, Zhongmin Zhang (nfzzm@163.com).

Materials availability

Reagents (including plasmids) generated in this study are available from the [lead contact](#).

Data and code availability

- All data reported in this paper will be shared by the [lead contact](#) upon request.
- This paper does not report original code.
- Any additional information required to reanalyze the data reported in this paper is available from the [lead contact](#) upon request.

EXPERIMENTAL MODEL AND STUDY PARTICIPANT DETAILS

Mouse model of IVDD

Twenty 3-month-old male WT mice were randomly selected as a control group (Ctrl group). Another thirty 8-week-old male WT mice and 30 male TG mice with the same age were randomly selected to construct the aged (18-month-old) mouse IVDD model (WT 18M group, TG 18M group). The model mice were provided a high-fat diet (10% arachidonic acid, 90% maintenance diet) and were housed in a pathogen-free environment with constant temperature and humidity until they were sacrificed. After the age of 18 months, the mice were euthanized and the IVD specimens (L3-L6 segments) were collected ($n = 80$). Twenty IVD specimens of the mice in WT 18M group and TG 18M group were analyzed by gas chromatography to calculate the PUFAs content and the n-6/n-3 PUFAs ratio. The method was described in a previous study.⁴⁶ The other specimens were used to detect the free iron content and evaluate the degree of IVDD ($n = 20$ per group). In addition, twenty 4-week-old male Sprague Dawley (SD) rats were sacrificed for the extraction of primary NP and AF cells. All animals were purchased from the Experimental Animal Center of Southern Medical University and the animal experiments were approved by the Animal Ethics Committee (No. 2020-0217).

METHOD DETAILS

Histochemistry, immunohistochemical staining and tissue quantitative analysis

IVD specimens were fixed, decalcified, dehydrated, paraffin-embedded, and processed into serial 4 μ m coronal sections. After deparaffinization and hydration, hematoxylin and eosin (H&E), Safranin O/Fast Green (SO/FG) and Masson staining were performed. For immunohistochemistry (IHC), slices were placed in citric acid solution (50mM) and incubated in a water bath at 60°C for 16 h to extract antigen, then incubated in 30% hydrogen peroxide solution for 10 minutes and blocked with 10% goat serum at 37°C for 1 hour. The sections were incubated in antibodies against MMP-13, OCN, NCOA4, LGR5 (purchased from ABclonal), Collagen X, p53, p16^{INK4A}, Ferritin, β -catenin (purchased from

Abcam), and Col2a1 (purchased from Millipore) at 4°C overnight, followed by incubation in secondary antibody (purchased from Abcam) for 1 hour at room temperature, DAB chromogenesis and hematoxylin staining. For IF staining, the sections were incubated with a secondary antibody (purchased from Abcam) followed by staining with DAPI. In the quantitative analysis, the CEP height was calculated by using the mean value of the CEP height at 25%, 50%, and 75% of the coronal position of the IVD. The degree of IVDD was scored according to the modified scoring method in the previous literature.⁴⁷ IHC and IF staining were performed to compare protein expression by calculating the positive cell ratio.

Cell culture and treatment

Because primary IVD cells of mice are difficult to culture, in this study, IVD cells derived from SD rats were extracted and cultured. After the 4-week-old rats were sacrificed, the caudal IVD was collected and placed in high-glucose Dulbecco's modified Eagle's medium. After the surrounding tissue was removed, the IVD was separated from the AF with a scalpel blade, the NP tissue was collected, and complete medium (10% fetal bovine serum, 1% streptomycin and penicillin, 1% L-glutamine) was added to culture the NP cells. The AF tissue was excised and transferred to another cell dish. The above operations were performed with a stereomicroscope. The AF tissue was digested with trypsin for 30 minutes and then digested with 0.2% type II collagenase for 4 hours. The cell suspension was collected and centrifuged at 1000 rpm for 5 minutes, the supernatant was discarded, and the cell pellet was washed three times with high-glucose medium. A 70- μ m tissue filter was added to the complete medium to culture the AF cells. The NP and AF cells were passaged after reaching 80% growth, the second passages were used for *in vitro* experiments.

The pcDNA3.1 plasmid overexpressing NCOA4 and LGR5 was synthesized by Guangzhou Laisai Biotechnology Company. Cells were transfected with plasmids using Lipo3000™ transfection reagent (Invitrogen, USA) at the final concentrations described by the manufacturer: 2 μ g/ml NCOA4 plasmid and 2 μ g/ml LGR5 plasmid. 48 hours after transfection, cells were treated with interleukin 1 β (IL-1 β , 10 ng/mL, 24 hours), deferiprone (DFO, 1 μ M, 24 hours), ferric ammonium citrate (FAC, 100 μ M, 24 hours), CAS-853220-52 (100 nM, 24 hours) or XAV-939 (1 μ M, 24 hours) treated cells.

Cell counting kit-8 (CCK-8) assay

The cells were seeded in a 96-well plate at a density of 5×10^3 . After 48 hours of adherence, the cells were treated with serum starvation and IL-1 β for 24 hours. Then different concentrations (0.5, 1, 2, 5, 10 nM) and durations (24, 48, 72 hours) of DHA were exogenously added. Cell viability was detected by CCK-8 (Dojindo, Japan) according to the manufacturer's protocol.

Cell cycle detection

The cells were trypsinized to collect adherent cells by pipetting and gently blowing off the cells. The cells were then centrifuged at 1000g for 3-5 minutes to pellet them, and the supernatant was discarded. After adding 1ml of PBS, the cells were centrifuged again. Fixation was achieved by adding 70% ethanol and incubating for 30 minutes. Propidium iodide staining solution was then added, and the cells were incubated in the dark at 37°C for 30 minutes. Flow cytometry detection was subsequently performed at a wavelength of 488nm. Data analysis according to the manufacturer's protocol (Beyotime, China).

SA- β -gal staining

Cells were seeded in 12-well plates at a density of 3×10^4 . After 48 hours of adhesion, cells were treated with serum starvation and IL-1 β for 24 hours. Then DHA (1 nM, 72 hours), DFO or FAC was added. SA- β -Gal staining was performed according to the manufacturer's protocol (Beyotime, China), and the positive cell ratio was calculated.

Free iron content assay

The IVD tissue proteins of mice in each group were collected. The IVD cells were treated with serum starvation and IL-1 β addition for 24 hours, followed by exogenous addition of DHA (1 nM, 72 hours). Then, the proteins of the cells in each group were collected. According to the manufacturer's protocol (Beyotime, China), the iron content was detected. The amount of protein was calculated using a BCA detection kit for normalization.

Malondialdehyde (MDA) content assay

The cells were seeded in 6-well plates at a density of 3×10^4 . After 48 hours of adherence, cells were treated with serum starvation and IL-1 β for 24 hours, and DHA (1 nM, 72 hours) or oe-NCOA4 (48 hours) was added exogenously. Then MDA detection was performed according to the manufacturer's protocol (Beyotime, China). The protein amount was calculated by a BCA detection kit for normalization.

Cytofluorescence assay

The cells were seeded in confocal dishes at a density of 10^4 for 48 hours. In the FerroOrange experiment, DHA (1 nM, 72 hours), oe-NCOA4 (24 hours), Wnt agonist, oe-LGR5 and XAV-939 were added exogenously to the cells after treated with serum starvation and IL-1 β for 24 hours. After fixation with 4% paraformaldehyde for 15 minutes, the cells were incubated with FerroOrange reagent (37°C, protected from light, 30 minutes), ferrous iron was observed by confocal microscopy, and the fluorescence intensity was calculated. In the IF experiment, DHA (1 nM, 72

hours), oe-NCOA4 (24 hours), and oe-LGR5 were exogenously added after serum starvation and IL-1 β (10 nM, 24 hours) treatment of cells. Fix with 4% paraformaldehyde for 15 minutes, block with 10% goat serum at 37°C for 30 minutes, the cells were then incubated with LC3II (purchased from CST), ferritin and β -catenin antibodies overnight at 4°C, followed by the secondary antibodies (purchased from Abcam) incubation for 1 hour at room temperature. After DAPI staining, protein expression was monitored by confocal microscopy. In the ROS fluorescence assay, the IVD cells were treated with serum starvation and IL-1 β addition for 24 hours, followed by exogenous addition of DHA (1 nM, 72 hours). Then, the cells were stained according to the manufacturer's protocol (Beyotime, China), the ROS level was detected. The Fluorescence intensity was calculated by the Image J (NIH, USA).

TEM assay

The cells were seeded in 6-well plates at a density of 3×10^4 . After 48 hours of adherence, cells were treated with serum starvation and IL-1 β for 24 hours, and DHA (1 nM, 72 hours) was added exogenously. Following digestion and centrifugation, the cells were fixed in 2.5% pentanediol at room temperature for 4 hours. Subsequently, the cells were washed with PBS and fixed with 1% osmium tetroxide for 2 hours at room temperature. Then, the cells underwent dehydration using graded alcohol and acetone. The cells were soaked according to the following steps: acetone/embedding solution (3/1) for 30 minutes, 100% acetone/embedding solution (1/1) for 4 hours, and pure embedding solution overnight at 4°C. After embedding, the samples were placed in an oven at 37°C for 24 hours, followed by 60°C for 48 hours. The samples were then cut into ultrathin sections with a thickness of approximately 100 nm using an ultramicrotome (Leica UC7, Germany). Finally, the sections were stained with uranyl acetate for 20 minutes and lead citrate for 12 minutes, and subsequently photographed using a transmission electron microscope (Tecnai G2 Spirit, USA).

qRT-PCR

Total RNA was extracted from cells using TRIzol reagent (Thermo, USA) according to the manufacturer's instructions. cDNA was synthesized from the extracted RNA using PrimeScript RT Master Mix (Takara, Japan). mRNA levels were determined by the SYBR green I incorporation method and real-time PCR system (Takara, Japan). Relative fold changes at the gene level were calculated using the $2^{-\Delta\Delta Ct}$ method. Primers were from Shanghai Bioengineering (Table S1).

Western blot

Total protein was extracted and dissolved in Laemmli solution (62.5 mM Tris-HCl, pH 6.8, 2% sodium lauryl sulfate, 10% glycerol, 50 mM di-thiothreitol, 0.01% bromophenol blue) at 95°C for 10 minutes. Proteins were separated by electrophoresis using sodium dodecyl sulfate-polyacrylamide gels and transferred to nitrocellulose membranes. The membranes were sealed in tris-buffered saline containing 5% skimmed milk and 0.1% Tween 20 at room temperature for 1 hour. Subsequently, the membrane was incubated with the primary antibodies against p53, p16^{INK4A}, p21, NCOA4, ferritin, β -catenin, GSK-3 β , p-GSK-3, LGR5, histone, β -actin overnight at 4°C. After that, the secondary antibody was applied at room temperature for 1 hour. An ultrasensitive ECL chemiluminescence kit was used to expose the bands, and the software was used to observe and analyze the bands.

QUANTIFICATION AND STATISTICAL ANALYSIS

Data analysis was performed using SPSS 25.0 software (SPSS, USA). Graphs were generated using GraphPad Prism 8 software (GraphPad, USA). The histological results and *in vitro* experimental data between each group were analyzed using one-way analysis of variance (ANOVA) followed by LSD. Data are presented as mean \pm standard deviation. Values of * $p < 0.05$; ** $p < 0.01$; *** $p < 0.001$ were considered statistically significant.